Mixed control for robust vibration isolation: numerical energy comparison for an active micro suspension device

Yann Meyer, Manuel Collet

Mixed control for robust vibration isolation: numerical energy comparison for an active micro suspension device

Y Meyer and M Collet

FEMTO ST Département LMARC, UMR 6174, F-25000 Besançon, France

An original control approach for robust vibration isolation is introduced in this paper. Two feedback signals, the relative displacement and the transmitted force between the sensitive element and its disturbing support, are employed in a so-called mixed control design. This strategy is used to perform control in the case of protection of electronic components, such as frequency generators, vibrating gyroscopes and certain accelerometers, essential to the operation of electronic cards. The simplicity of the control law allows us to tune the parameters of the controller with a very simple optimization process. The proposed isolation control is implemented and optimized for a micromechanical piezocomposite structure and the performance and the energy cost are compared with those of integral sliding control and LMI-optimized control.

1. Introduction

Vibration isolation is necessary in two broad classes of problems:

- a vibrating element is fixed on a structure. The waves can move into this whole structure. Thus, they can damage the different sensitive elements of the structure or reduce their service life.
- a sensitive element is fixed on a vibrating structure. So, the vibrations can modify the operating points of this element but also damage it strongly.

Due to these problems, limiting the vibration transfer between an element and its support becomes very attractive. In fact, the objective of vibration isolation is to limit vibration energy flow between two structures. The idea is to create a mechanical connection which allows the greatest operation of sensitive elements, such as electronic components. In a vibratory environment, the good operation of electronic components, such as frequency generators, vibrating gyroscopes and certain accelerometers, are essential to the operation of electronic cards. In this paper, one way to protect them against hazardous vibrations is studied.

Passive vibration isolation is the simplest way to achieve this goal. Several passive techniques have been studied in the literature such as the use of elastomer materials, shape memory alloys or modifying the mechanical impedance [1–4].

The passive suspension described in figure 1 is considered.

The transfer function of the system, i.e. the relationship between the acceleration of the mass ($\ddot{W}_\mathrm{s}$) and the acceleration imposed on the support ($\ddot{W}_\mathrm{u}$) is written in Laplace variables:

$$T_{\ddot{W}_\mathrm{s},\ddot{W}_\mathrm{u}} = \frac{(\ddot{W})_\mathrm{s}}{(\ddot{W})_\mathrm{u}} = \frac{sC+K}{s^2M+sC+K} \tag{1}$$

with

K: the stiffness of the suspension (in N m^{-1}),
M: the mass of the structure (in kg),
C: the damping produced by the suspension (in kg s^{-1}). (2)

The objective of any suspension is obviously to limit the acceleration of the system to be isolated in the required

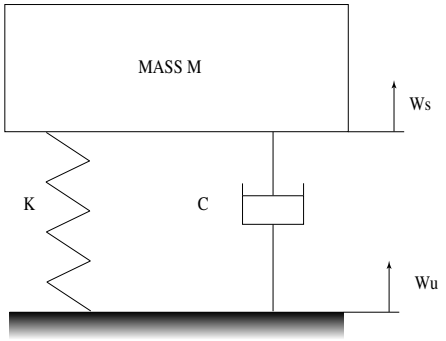

Figure 1. 'Mass-Spring-Damper' system.

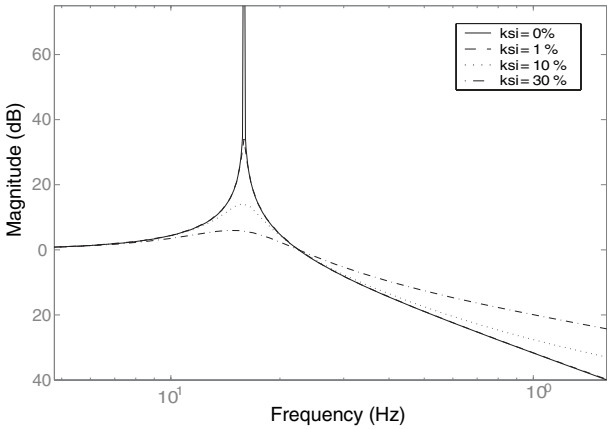

Figure 2. Evolution of the transfer function for different values of $\xi = \frac{C}{2}\sqrt{(\frac{M}{K})}$.

frequency bandwidth. The behavior of the system is observed in figure 2 where different transfer functions are plotted for different values of the reduced damping ratio $\xi = \frac{C}{2}\sqrt{(\frac{M}{K})}$.

As shown in figure 2, this system presents a modal resonance peak, that is to say an increase of the acceleration of the system to be isolated in a narrow frequency bandwidth. Obviously, modal peaks attenuate when the damping ratio of the system is increased. Consequently, the resonance amplification is decreased and the sensitive mass stability increases in the narrow frequency bandwidth around the considered eigenfrequency. However, this effect also results in a reduction of the high frequency filtering decay rate. Indeed, this high frequency decay rate evolves from -40 dB/decade when no structural damping is considered in the suspension to -20 dB/decade when ξ is non-null with an amplification shift proportional to this value. It results also in poor isolation in this frequency range. It also becomes necessary to lower the cutoff frequency to increase the high frequency isolation capability of the suspension. This modification is performed by limiting the stiffness of the connection, which involves a loss of stability in low frequencies. Ultimately, the traditional mechanical compromise is in the ratio between the stiffness and the damping of the connection [1].

The best mechanical compromise can be obtained by using an active control process [1]. Sky-hook control is the simplest and most common control strategy [5]. This isolation method is stable and robust. The idea is to introduce actively, in the mechanical connection, a viscous damper rigidly fixed to a stationary coordinate system. The design of this controller is based on an absolute sensing signal such as acceleration, transmitted force, absolute velocity or absolute displacement. The studies of various sky-hook-type strategies are broadly proposed in the literature [6]. These isolation techniques are highly efficient and robust for operating frequencies over the resonance peak of suspension. However, for design constraints, actively modifying the mechanical connection at frequencies below the resonance peak of suspension can be necessary. Indeed, in the micromechanics field, the small dimensions of structures do not allow us to decrease the resonance peak of suspension for reasons of the strength of materials. So research on isolation control for large frequency bandwidths have been carried out. In these control strategies, the control laws are computed by strong mathematical processes such as sliding surface methods [7–9] or LMI-optimized control [10–13]. Let us note that the methods of reduced order control [11] cannot be directly applied when a feedthrough term is present in a state–space model of the studied device, like when transmitted force or acceleration are picked up. In this paper, an original and simple control approach for robust vibration isolation is introduced. Two feedback signals, the relative displacement and the transmitted force between the sensitive element and its disturbing support, are employed in a 'mixed' control strategy. Indeed, the measurement of a primal quantity such as relative displacement is mixed with the measurement of a dual quantity such as acceleration to provide a mixed set of inputs in the proposed control strategy. This strategy is used to perform large frequency bandwidth control. An energy comparison with other control techniques is also performed. Indeed, in micromechanical devices, the limited power of actuators, the problems of electronic operation and the power perturbations of electronics indicate that control energy becomes a crucial design parameter.

This paper is organized as follows. In section 2, the description and the modeling of the micromechanical piezocomposite structure studied are given. At the end of this section, the state–space model for active suspension is introduced. This section is the basis for the numerical implementation of the mixed isolation control in section 3. The efficiency and the energy cost of this control strategy are compared with those of integral sliding control [9] and LMI-optimized control [11] in section 4. Finally, concluding remarks are given in section 5.

2. Modeling of the micro suspension device

An active suspension system made of silicon and piezoelectrically transduced is considered (cf figure 3). A silicon clamped–clamped cross is used as the basic passive structure on which the element to be isolated is located [14]. The active function is conferred to the structure by two piezoelectric actuators and three piezoelectric sensors deposited on the top face of the cross. These active parts of the system are founded on thin PZT-type layers [15]. Thus, the direct and opposite piezoelectric effects are used. In order to simultaneously allow detection and activation, a multielectrode system was designed. The actuators are placed near the boundaries of the main beam and

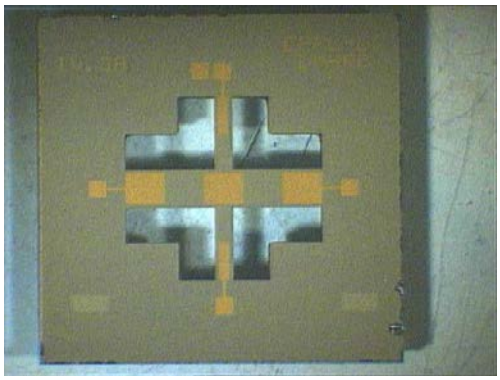

Figure 3. Photograph of the suspension device.

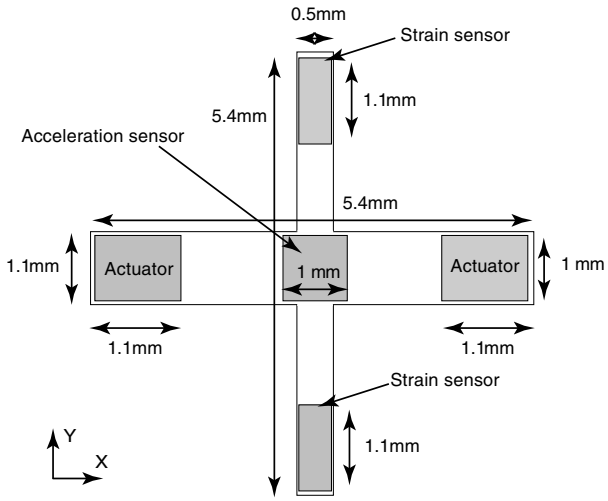

Figure 4. Dimensions of the device.

their length is optimized in order to obtain the maximum action force on the first natural mode [16, 17]. On the transversal beam, two layers are used as strain sensors, that is to say as displacement sensors. An acceleration sensor is also located on the middle of the suspension. It constitutes the support of the sensitive element, in our case, a small mass made of steel (7.9 mg). In figures 4 and 5, the dimensions of the device are presented. The device is considered as a pseudo-collocated system in a large frequency bandwidth because of its small dimensions and the induced in-phase responses of its actuators and sensors set-up. Collocated strategies guarantee the asymptotic stability of the closed-loop system. This property is a consequence of the systematic introduction of energy dissipation into the structure via the controller. A robust damper is added to the structure by the collocated strategies. The stability and the robustness of the system are thus guaranteed under the sensible assumption that the control force is applied instantaneously [1].

The numerical model employed is a multiphysics finite element model developed under the Femlab software. For the FE discretization of the model, the automatic mesher of Femlab is used. In the 2D space (plan ZX), the Argyris' finite elements are used [18]. The 2D space is considered in order to account for the shear effect in the piezoelectric film [19, 20].

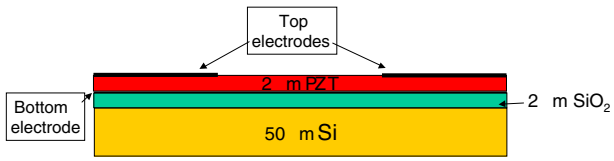

Figure 5. Thickness of the different films of the suspension device.

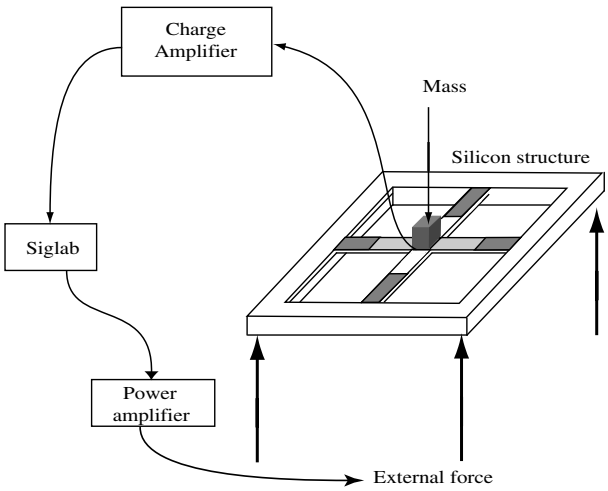

Figure 6. Experimental verification architecture.

The modeling of the system was based on piezoelectric theory, so on a linear theory [21, 22]. For modeling, only the first natural mode of the device is considered (cf. figure 8). Indeed, the system induces an active isolation only along one single degree of freedom (the Z axis) of the electronic system to be stabilized. So, the acceleration forces on the sensitive system are only applied along the Z axis and the natural suspension mode is supposed to be the major device response. The diagram of the experimental verification of the single-mode model hypothesis is shown in figure 6. The input of external forces applied to a seismic mini-table (especially manufactured for this application) is generated by a Siglab plate-form. This Siglab plate-form is also placed for acceleration measurement purposes.

In figure 7, the experimental Bode diagram between the output signal from the acceleration sensor and the signal applied to the actuators of the seismic table is presented. Experimental results show that a large frequency bandwidth is dominated by the vibrational response of only the first natural mode.

The inherent damping factor is considered small ($\xi = 0,1\%$) because the materials used (silicon and PZT) are brittle.

The first projected equation of motion around the equilibrium state is written as:

$$M\ddot{w}_s + C(\dot{w}_s - \dot{w}_u) + K(w_s - w_u) - u(w_u, w_s) = 0 \quad (3)$$

with M the mass of the sensitive element, C the damping coefficient, K the stiffness coefficient, w_s the first mode displacement of the sensitive element, w_u the displacement of the support and $u(w_u, w_s)$ the control force.

Moreover, the control device has two types of sensor:

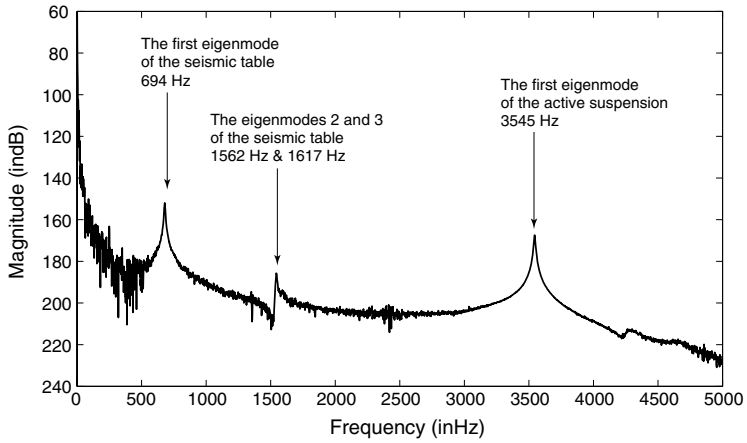

Figure 7. Experimental Bode diagram between the output signal from the acceleration sensor and the signal applied to the actuators of the seismic table.

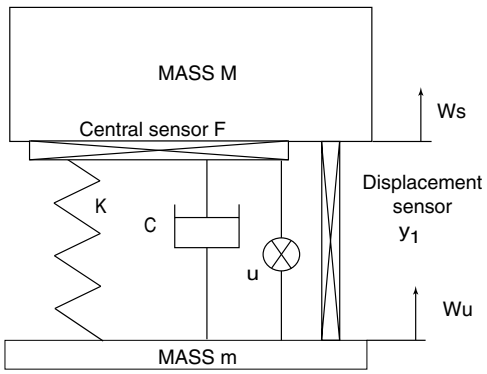

Figure 8. Isolation system based on mixed vibration control.

- the first sensor behaves as a relative displacement sensor located between the moving mass and the support. So, the signal $y_1(t)$ is

$$y_1(t) = \alpha(w_s(t) - w_u(t)) = \alpha w(t) \tag{4}$$

  where α is the sensing factor.
- the second sensor is an effort sensor. The measured signal $F(t)$ is written:

$$F(t) = \beta M \ddot{w}_s = \beta(-C\dot{w}(t) - Kw(t) + u(w_u, w_s)) \tag{5}$$

  where β is the sensing factor. We can also underline the feedthrough term in this measurement is directly linking the control signal $u(w_u, w_s)$ into the output signal carried out.

So, the reduced state–space model of the suspension is built with the tension applied to the actuators and the acceleration applied to the device as input signals and the signals of the sensors and the absolute acceleration endured by the sensitive element as output signals.

The state–space representation can be expressed as follows, according to equations (3)–(5):

$$\begin{Bmatrix} \dot{w} \\ \ddot{w} \end{Bmatrix} = A \begin{Bmatrix} w \\ \dot{w} \end{Bmatrix} + B \begin{Bmatrix} u(w_u, w_s) \\ \ddot{w}_u \end{Bmatrix} \tag{6}$$

Table 1. Parameters of the experimental device expressed on its first natural mode.

M (in g)	7.9
K (in N m^{-1})	4.9×10^6
ξ (in %)	0.1
α	0.062
β	1

with

$$A = \begin{bmatrix} 0 & 1 \\ -M^{-1}K & -M^{-1}C \end{bmatrix} \tag{7}$$

and,

$$B = \begin{bmatrix} 0 & 0 \\ M^{-1} & -1 \end{bmatrix}. \tag{8}$$

The equation of observation can be written:

$$\begin{Bmatrix} y_1(t) \\ F(t) \\ \ddot{w}_s \end{Bmatrix} = C \begin{Bmatrix} w \\ \dot{w} \end{Bmatrix} + D \begin{Bmatrix} u(w_u, w_s) \\ \ddot{w}_u \end{Bmatrix} \tag{9}$$

where

$$C = \begin{bmatrix} \alpha & 0 \\ -\beta K & -\beta C \\ -M^{-1}K & -M^{-1}C \end{bmatrix} \tag{10}$$

and

$$D = \begin{bmatrix} 0 & 0 \\ \beta & 0 \\ M^{-1} & 0 \end{bmatrix}. \tag{11}$$

The experimental parameters of the suspension device are given in table 1. They represent equivalent mechanical values on the first natural mode of the system. The value of the first frequency is 3545 Hz. These equivalent values are used in the following numerical simulations.

3. Mixed isolation control

3.1. Control law

The aim of vibration isolation systems is to protect sensitive elements by limiting the vibration transfer between this element and its support, that is to say, in a perfect case, to obtain $\ddot{w}_s = 0$. According to (3), a control force $u(w_u, w_s) = C\dot{w}(t) + Kw(t)$ is an ideal solution. Nevertheless, this control law is not robust and highly unstable in the Lyapunov sense [23, 24]. Indeed, the controller tries to remove the mechanical connection. Consequently, the relative displacement of the sensitive element is increased and leads to instabilities for high control gains.

The idea of our construction logic is to take advantage of the removing of the mechanical connection. A 'numerical' connection is introduced, in the precedent control strategy, by using a sky-hook-type feedback thanks to the effort sensor. With this pseudo-collocated feedback introduction, the control is stable [1]. So, two feedback signals, the relative displacement and the transmitted force between the sensitive element and the disturbing structure, are employed in a design called mixed control design. According to (3)–(5), the control force can be established as:

$$u(w_u, w_s) = Ky_1 + C\dot{y}_1 - \frac{C_{new}}{M}\int_0^\infty F(t)\partial t - \frac{K_{new}}{M}\int_0^\infty\int_0^\infty F(t)\partial t \quad (12)$$

where C_{new} and K_{new} are, respectively, the damping and stiffness coefficients of the desired mechanical connection. The choice of C_{new} and K_{new} is absolutely not crucial for the efficiency of the mixed control strategy. Indeed, all the external forces come by the support. So, the first part of the control force $C\dot{w}(t) + Kw(t)$ breaks the mechanical connection between the support and the element to be isolated. The sky-hook-type part of the control force $-\frac{C_{new}}{M}\int_0^\infty F(t)\partial t - \frac{K_{new}}{M}\int_0^\infty\int_0^\infty F(t)\partial t$ introduces a 'numerical' connection fixed to a stationary coordinate system. In an ideal case, the numerical connection will never see the external vibration So, we make the choice of $C_{new} = C$ and $K_{new} = c^2K$ where c is a tuning parameter.

The control force, defined in (12), cannot be implemented directly in a DSPace plate-form for the experiments. Indeed the direct integration algorithm is not physically realizable because of poles located at 0. So it is necessary to introduce high pass filters, avoiding constant signal unstable integration. So, it becomes necessary to avoid this part in the frequency scale of control. Consequently, various transfer functions, in Laplace variables, are used:

- an integration-type filter at first order:

$$I(s) = \frac{1}{s+a} \quad (13)$$

- a derivative-type filter at first order:

$$D(s) = \frac{s}{s+b} \quad (14)$$

- a transfer function to avoid the bias of signals:

$$PH(s) = \frac{s}{s+a} \quad (15)$$

where a, b are design parameters of control.

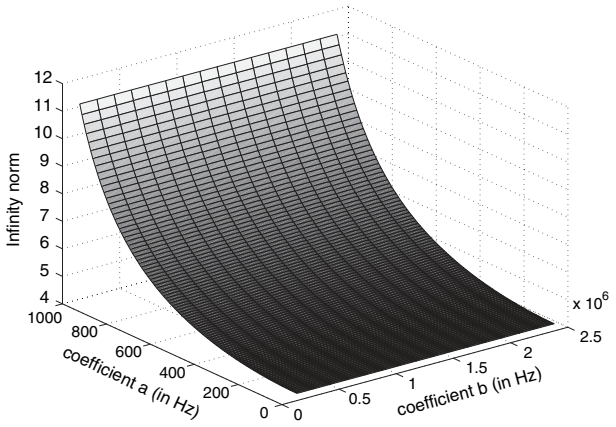

Figure 9. H_∞ Norm of $T_{\ddot{w}_s,\ddot{w}_u}$ as a function of the parameters a and b.

With equations (13)–(15), the control force (12) is expressed as:

$$u(w_u, w_s) = \mathrm{TF}^{-1}\left(PH(s)\left[K\tilde{y}_1 + CD(s)\tilde{y}_1 - \frac{C_{new}}{M}I(s)\tilde{F} - \frac{K_{new}}{M}I(s)I(s)\tilde{F}\right]\right) \quad (16)$$

with TF^{-1} the inverse Laplace transformation and $\tilde{x}$ the Laplace transformation of $x(t)$.

3.2. Optimization process and numerical results

The design parameters have to be optimized in order to minimize the absolute acceleration $\ddot{w}_s$ and the control energy cost for a random disturbance with an intensity value of 1 g (9.81 m s^{-2}). The value $u(w_u, w_s)$ being proportional to the value $\ddot{w}_u$, the values of energy consumption of control can be simply computed. The objective functions are the H_2 and H_∞ norms of the different transfer functions [24]. The choice of optimization type depends on the performance requirement and the disturbance. Generally, for a state–space model, H_2 optimization is used to optimize the energy of the output signal for a random disturbance, that is to say to obtain the best performance in a large frequency bandwidth, and H_∞ optimization is used to optimize the maximal amplitude value of the output signal, that is to say to obtain the best performance in a narrow frequency bandwidth. The optimization process is performed under the Matlab environment.

The optimization process is carried out in two steps. The first step concerns the determination of the high frequency cutoff parameter b. As shown in figures 9 and 10, this coefficient has no effect on the H_2 and H_∞ norms of $T_{\ddot{w}_s,\ddot{w}_u}(a, b, c)$ if it is chosen so that $b \gg 3545$ Hz, and thus for a large set of c values, including those obtained at the end of the optimization process. Arbitrarily, we can fix it equal to $b = 1.5 \times 10^5$ Hz. By fixing this roll-off frequency, which has no influence on the used criterion, we simplify the numerical complexity of our optimization.

Once the parameter b is fixed, the parameters a and c are considered for the second optimization loop. The

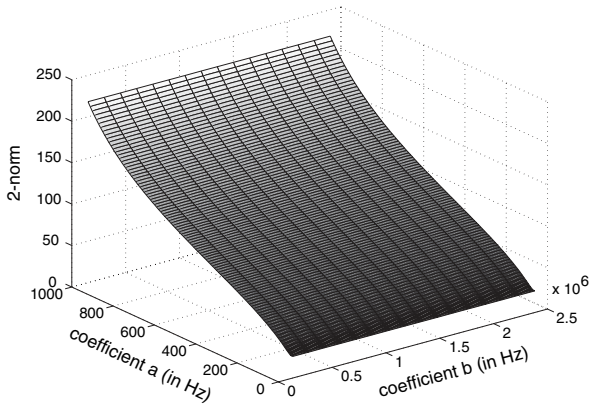

Figure 10. H_2 Norm of $T_{\ddot{w}_s,\ddot{w}_u}$ as a function of the parameters a and b.

Table 2. Optimal values of the design parameters a and c for H_2 and H_∞ optimization processes (b is chosen equal to 1.5×10^5 Hz.).

	Parameter a (in Hz)	Parameter c (without unit)
H_2 optimization	610	0.75
H_∞ optimization	700	0.75

H_2 and H_∞ norms of the function $T_{\ddot{w}_s,\ddot{w}_u}$ $(a, b = 1.5 \times 10^5, c)$. $T_{u(w_s,w_u),\ddot{w}_u}$ $(a, b = 1.5 \times 10^5, c)$, which represent the objective functions, are optimized to obtain the best compromise between efficiency and control energy flow. In figures 11 and 12, the response surfaces for, respectively, the H_∞ and H_2 optimization processes, are presented.

Thanks to the optimization loops, the optimal values of design parameters a and c are found for H_2 and H_∞ optimization and presented in table 2.

In figures 13 and 14, the relation between the absolute input acceleration $\ddot{w}_u$ and the absolute output acceleration $\ddot{w}_s$ is shown for the H_∞ and H_2 optimizations. The responses of the controlled and uncontrolled systems are compared.

It can be observed that the first natural mode is strongly attenuated (cf table 4) for both optimizations. Moreover, the high frequency isolation is improved. Indeed, the value of the high frequency decay rate is around -60 dB/decade just after the resonance peak. This value is unreachable with a simple collocated control. Figures 13 and 14 indicates also, by the dashed line, the control force evolution. In table 3, a energy comparison is presented. With an H_2 optimization, it makes it possible to improve the isolation capabilities of the system for a large frequency bandwidth. That is why the energy cost of a H_2 optimized controller is most important.

Table 3. Energy comparison of the performance obtained for the mixed control applied to the studied device with H_2 and H_∞ optimization.

	H_2 norm control force	H_∞ norm control force	Maximum control power (in μW)
H_2 optimization	7.85	0.19	51.1
H_∞ optimization	6.95	0.15	42.5

Table 4. Comparison of the performance obtained for the different optimized vibration control strategies for 1 g random disturbance.

	H_2 norm	H_∞ norm	Damping ratio (in %)
Free system	2492.8	500	0.1
Mixed control (H_2 opt.)	138.8	2.5	13.5
Mixed control (H_∞ opt.)	162	2.8	16.1
Integral sliding control	101.22	4.19	23.2
LMI-optimized control (H_2 opt.)	32.9	1	100
LMI-optimized control (H_∞ opt.)	3.78	48.1	1

The interest of the mixed control strategy is to limit $\ddot{w}_s = 0$ without creating instabilities due to an excessive relative displacement of the sensitive element. In figures 15 and 16, the relation between the absolute input acceleration $\ddot{w}_u$ and the relative displacement y_1 is presented for the H_∞ and H_2 optimizations. It can be observed that there is an increase of the relative displacement level around the frequency where the mechanical connection is modified. But this amplification is limited.

4. Numerical comparison

For the efficiency and energy comparison, two other different vibration control strategies are selected for their robustness and

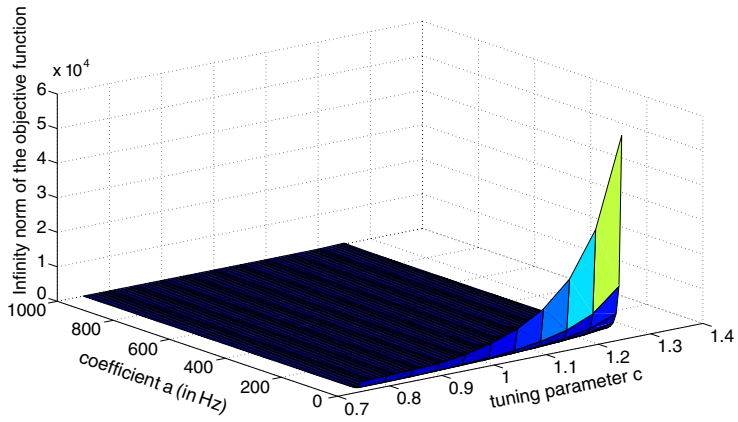

Figure 11. H_∞ Norm objective function versus the parameters a and c.

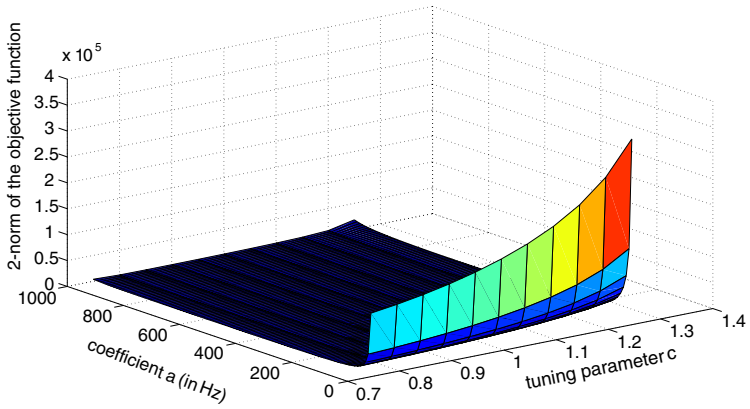

Figure 12. H_2 Norm objective function versus the parameters a and c.

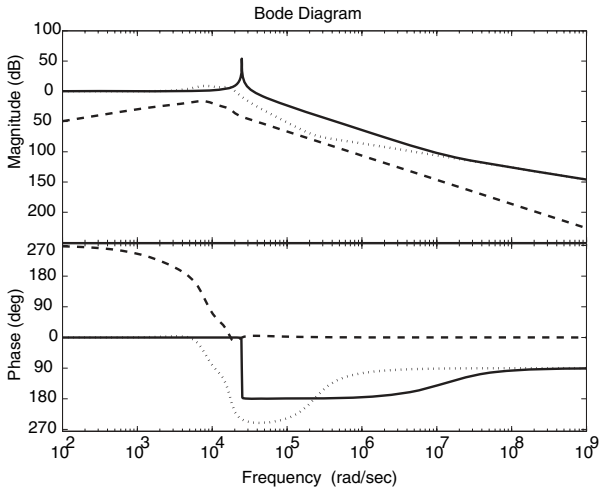

Figure 13. Bode diagrams of $T_{\ddot{w}_s,\ddot{w}_u}$ for the free system (solid line) and for the controlled system with the H_∞ norm optimized controller (dotted line). The dashed line shows the associated control force.

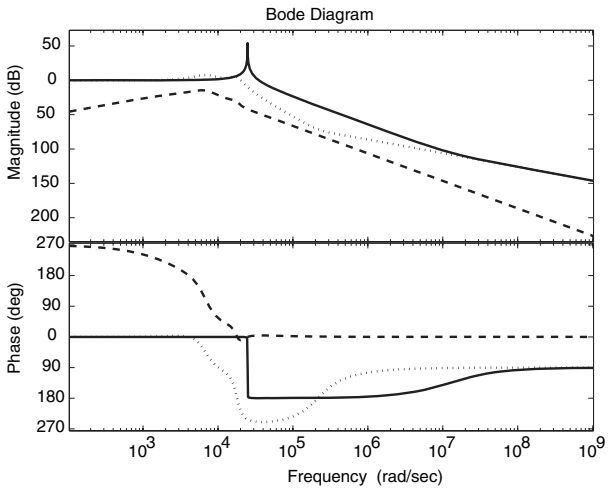

Figure 14. Bode diagrams of $T_{\ddot{w}_s,\ddot{w}_u}$ for the free system (solid line) and for the controlled system with the H_2 norm optimized controller (dotted line). The dashed line shows the associated control force.

Table 5. Energy comparison of the performance obtained for the different optimized vibration control strategies for 1 g random disturbance.

	H_2 norm control force	H_∞ norm control force	Maximum control power (in μW)
Mixed control (H_2 opt.)	7.85	0.19	51.1
Mixed control (H_∞ opt.)	6.95	0.15	42.5
Integral sliding control	1.01	22.6	891.6
LMI-optimized control (H_2 opt.)	503.2	239.3	52 000
LMI-optimized control (H_∞ opt.)	3.78	7.83	14.1

performance properties: integral sliding control [9] and LMI-optimized control [11]. In the case considered, the structure is excited with a 1 g random disturbance. The controllers are optimized for the best damping ratio and the lowest energy cost. All the optimization processes were computed under Matlab software. SeDuMi 1.04 freeware is used for LMI optimization [25].

For the optimization processes of the classical vibration control strategies, the feedthrough term, introduced by the acceleration measurement, is removed in the state–space equations. This term induces instabilities in the computation of the norms [11]. Let us note that, in the optimization process of the mixed isolation strategy presented in section 3, measurement with a feedthrough term is used with no problem of stability.

In figure 17 and in table 4, H_2 LMI-optimized control appears as the best vibration isolation control for efficiency. But this performance has a very high energy cost (cf table 5). On the opposite side, the energy cost of H_∞ LMI-optimized control is very low and high frequency decay rate is around -60 dB/decade. The problem is the large amplitude at cutoff frequency. Indeed, the initial damping is lightly increased but not significantly.

So, the last comparison step is between mixed controls and integral sliding control. In figure 17 and in table 4, the damping ratio reached by the integral sliding mode strategy is better than the one from mixed controls on the suspension frequency. Unfortunately, another amplification peak is observed in the

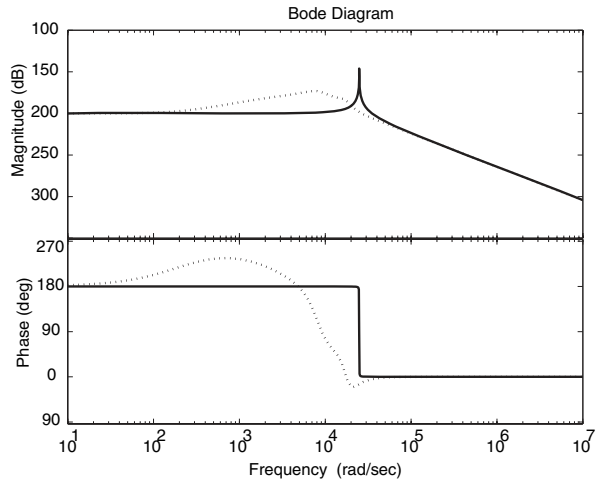

Figure 15. Bode diagrams of $T_{y_1,\ddot{w}_u}$ for the free system (solid line) and for the controlled system with the H_∞ norm optimized controller (dotted line).

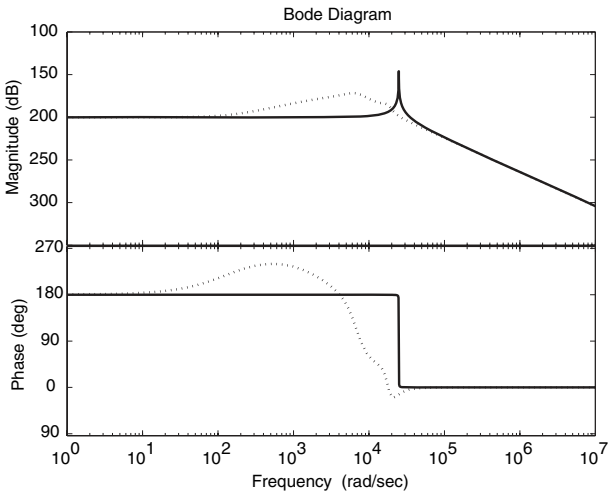

Figure 16. Bode diagrams of $T_{y_1,\ddot{w}_u}$ for the free system (solid line) and for the controlled system with the H_2 norm optimized controller (dotted line).

low frequency bandwidth. Moreover, the energy cost of mixed controllers is a great advantage. In fact, the mixed approach is the greatest compromise between energy cost and efficiency. The simple implementation is another advantage of these engineering laws.

5. Concluding remarks

In this paper, a new robust vibration control is proposed to achieve vibration isolation. This control is based on a signal mixing relative displacement and transmitted forces between a sensitive element and its disturbing structure.

The energy and performance comparison between two robust and stable vibration isolation strategies and the mixed controls demonstrated numerically the large capacities of the mixed approach. Moreover, this strategy does not need a heavy mathematical background to implement a controller

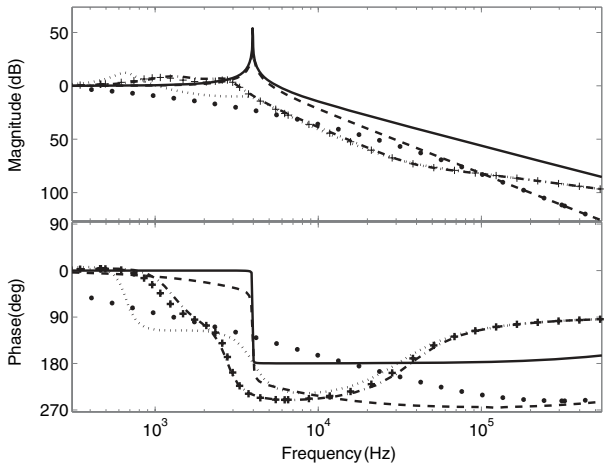

Figure 17. Bode diagrams of $T_{\ddot{w}_s,\ddot{w}_u}$ for the free system (solid line), for the controlled system with the integral sliding controller (dotted line), for the controlled system with the H_{inf} norm LMI-optimized controller (dashed line), for the controlled system with the H_{inf} norm optimized mixed controller (dashed–dotted line), for the controlled system with the H_2 norm optimized mixed controller (plus signs) and for the controlled system with the H_2 norm LMI-optimized controller (circles).

based on the mixed approach. Moreover, this strategy allows the introduction of measurements with feedthrough terms with no stability problems.

The following research is on the experimental implementation of the mixed vibration control. The manufacturing feasibility of micro suspension devices has already been shown in [26]. Before demonstrating experimentally the concept of 'small isolation islands', difficulties, due to the complex electrode configuration and the existence of the inevitable bottom electrode common to actuating layers and sensing layers, have to be completely managed [27].

References

[1] Preumont A 2002 *Vibration Control of Active Structures: An Introduction* (Dordrecht: Kluwer–Academic)

[2] Zak A, Ostachowicz W and Krawczuk M 1998 Buckling of a multilayer composite plate with embedded shape memory alloy fibers *Proc. ICCE/5 (Las Vegas)*

[3] Bernhard R, Ith W and Chiu G 1999 Passive-adaptative vibration absorbers using shape memory alloys *SPIE Conf. on Smart Structures and Integrated Systems (Newport Beach)* pp 63–641

[4] Knowles J K and Abeyaratne R 1999 On a shock-induced martensitic phase transition *J. Appl. Phys.* **87** 1123–34

[5] Karnopp D C and Trikha A K 1969 Comparative study of optimization techniques for shock and vibration isolation *Trans. ASME, J. Eng. Ind.* **91** 1128–32

[6] Preumont A, François A, Bossens F and Abu-Hanieh A 2002 Force feedback versus acceleration feedback in active vibration isolation *J. Sound Vib.* **257** 605–13

[7] Slotine J J 1983 Tracking control of non-linear systems using sliding surfaces *Thesis* Massachusetts Institute of Technology

[8] Slotine J J 1984 Sliding controller design for nonlinear systems *Int. J. Control* **40** 421–34

[9] Zuo L and Nayfeh S A 2004 An integral sliding control for robust vibration isolation and its implementation smart structures and materials: damping and isolation *Proc. SPIE* **5386** 1–10

[10] Gahinet P and Apkarian P 1994 A linear matrix inequality approach to H_∞ control *Int. J. Robust Nonlinear Control* **4** 421–48
[11] Tanaka H and Sugie T 1999 New characterization of fixed-order controllers based on LMI *Int J. Control* **72** 58–74
[12] Masubushi I, Ohara A and Suda N 1995 LMI-based output feedback controller design *Proc. ACC* pp 3473–7
[13] Chilali M and Gahinet P 1996 H_∞ design with pole placement constraints: an LMI approach *IEEE Trans. Autom. Control* **41** 358–67
[14] Meyer Y, Collet M and Delobelle P 2004 Active damping of electronic microcomponents with piezoelectric MEMS devices *Cansmart 04 Int. Workshop Smart Materials and Structures (Montréal)*
[15] Ledermann L, Muralt P, Baborowski J, Gentil S, Mukati K, Cantoni M, Seifert A and Setter N 2003 {100}-textured, piezoelectric $Pb(Zr_x, Ti_{1-x})0_3$ thin films for MEMS: integration, deposition and properties *Sensors Actuators* A **105** 162–70
[16] Monnier P, Collet M and Piranda J 2005 Definition of mechanical design parameters to optimize efficiency of integral force feedback *Struct. Control Health Monitor.* **12** 65–89
[17] Meyer Y, Collet M and Delobelle P 2007 Primal–dual optimization process of IFF-DVF active damping strategies. Applications to the beams *Struct. Control Health Monitor.* **14** 660–80
[18] Argyris J, Tenek L and Olofsson L 1997 TRIC: a simple but sophisticated 3-node triangular element based on 6 rigid-body and 12 straining modes for fast computational simulations of arbitrary isotropic and laminated composite shells *Comput. Methods Appl. Mech. Eng.* **145** 11–85
[19] Benjeddou A and Deü J-F 2002 A two-dimensional closed-form solution for the free-vibrations analysis of piezoelectric sandwich plates *Int. J. Solids Struct.* **39** 1463–86
[20] Fernandes A and Pouget J 2003 Analytical and numerical approaches to piezoelectric bimorph *Int. J. Solids Struct.* **40** 4331–452
[21] Banks H T, Smith R C and Wang Y 1996 Smart material structures: modeling, estimation and control *Research in Applied Mathematics* (Paris: Wiley–Masson)
[22] Lee C K 1990 Theory of laminated piezoelectric plates for the design of distributed sensors/actuators. Parts I and II *J. Acoust. Soc. Am.* **87** 1144–57
[23] Lee E B and Markus L 1967 *Foundation of Optimal Control Theory* (New York: Wiley)
[24] de Larminat P 1993 *Traité des Nouvelles Technologies* (Paris: Hermes) (Text in French)
[25] Peaucelle D, Henrion D and Labit Y 2001 *User's Guide for SeDuMi Interface 1.01: Solving LMI Problems with SeDuMi.* (Rapport LAAS n 01445)
[26] Meyer Y 2005 Controle actif de micro-composants electroniques *PhD Thesis* University of Franche-Comté (Text in French)
[27] Meyer Y, Verdot T, Collet M, Baborowski J and Muralt P 2007 Active isolation of electronic micro components with piezoelectrically-transduced silicon MEMS devices *Smart Mater. Struct.* **16** 128–34